Chapter 2

Current status of cosmic ray mass composition obtained by indirect measurements

2.1 Introduction

Knowledge of the CR mass composition is essential to the solution of the long existing enigma about their origin. The mass composition of CRs can strongly affect the acceleration and propagation processes from their accelerator sites. There was a serious note by Ginzburg and Syrovatskii - "It is very clear that any theory of the origin of CRs cannot expect serious success unless it rests on a detailed analysis of their mass composition from observed data" [1].

Observed CR data indicate that the CR energy spectrum contains about three to four structures: first, a *knee* around 3 or 4 PeV just after which the spectral index suddenly takes a value -3.1 from -2.7; *second knee* at an energy of roughly 0.4 EeV where a change in the spectral index occurs by $\Delta\gamma \approx -0.3$ arising out of the change in γ from roughly -3.0 to -3.3; an *ankle* in the vicinity of the few EeV energy after which the spectrum flattens again to its original slope; lastly, at energies above 40 EeV, the CR flux experiences a suppression, called the GZK effect [2–4]. In the vicinity of these spectral structures any measurement of the CR mass composition is expected to give important clues to the origin of these spectral features. On the other hand, the interaction cross-section, multiplicity and elasticity of the interactions in the atmosphere may differ from one type to

another type of the EAS initiating particle. Hence, the CR mass composition is very essential not only for exploring interesting astrophysical phenomena, but also for systematic studies of high-energy hadronic interactions.

This is not a task of one CR experiment or by a single thesis to make a complete study on the mass composition around the vicinities of all the spectral structures in the CR energy spectrum. In this thesis we have presented a number of studies exploiting different detection techniques for an EAS with some relatively new EAS observables particularly around the *knee* energy region.

2.2 EAS observables sensitive to cosmic ray mass composition

An EAS induced by a CR particle with energy roughly above 10^{14} eV provides a great amount of information about its type, energy, direction etc. Any detection of an EAS by means of ground based detector-system supplies directly information on arrival times and densities of cascade particles. The arrival direction of an EAS can be obtained with a fitting procedure applied to arrival times of EAS charged particles/electrons using an equation of a plane shower front. The EAS core position as well as the shower size ($\mathrm{N_{Ch}}$/$\mathrm{N_e}$) or shower age etc. can be obtained by fitting the lateral density, as obtained from the detector signal, with some suitable LDF from a variety of available LDFs; such as the NKG, the Greisen or the Hillas function. Almost the same data analysis method can be applied to other type of data obtained from atmospheric Cherenkov detector system. Likewise, event reconstruction based on signals/data obtained from atmospheric fluorescence measurements and radio emission detector arrays can also be done to obtain basic shower parameters.

Analyzing directly accessible EAS data (viz. density, arrival time etc. of secondary particles of an EAS) the basic EAS observables (viz. shower size, zenith angle, muon size, shower age, the depth of shower maximum, the EAS core location etc.) can be obtained. Now the information about the nature of the EAS initiating primary particle cannot be easily determined with the help of these basic EAS observables.

2.2.1 EAS observables from particles at ground

The measurement of particle densities of EASs at ground level is a frequently used approach of detecting CRs. Ground-based measurements offer very good geometric acceptance and high duty cycle to particle detectors in an EAS array. This approach also exhibits more susceptibility to shower-to-shower fluctuations. The combination of the Heitler and superposition models one relates the electron

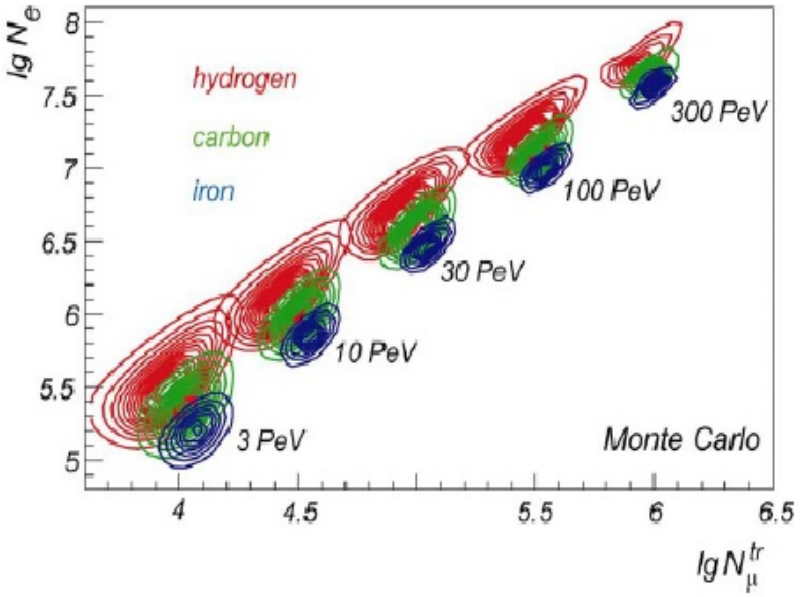

FIGURE 2.1: The electron size vs muon size distribution from simulated data for vertical showers at KASCADE level. Regions shown by contour lines meaning an inclusion of 90% of the showers (figure is taken from [5]).

size at shower maximum with CR energy, independent of the mass composition, whereas the muon size can be used to identify the mass of the CR particle. Under the above consideration, it is found that the variation of the muon size with increasing CR energy acts as a tracer of changes in the CR mass composition. But none of the detectors in an array can observe electron size at shower maximum in an experiment. One can therefore observe the attenuated electron size well below the point of shower maximum. It is known that heavy nuclei reach their shower maxima at smaller atmospheric depths than lighter ones. It is then obvious that the electron size would be larger for EASs initiated by lighter nuclei including proton. Hence the electron size is expected to be composition sensitive. A simulation study of the variation of electron size with muon size is shown in Fig.2.1 at some average energies [5]. The curve clearly shows that the mass composition

of CRs is correlated with the EAS electron size. Furthermore, the fluctuations of the electron and muon sizes are also used to determine the CR mass composition.

The LDF which is being used for EAS reconstruction, the corresponding shape of the LDF is expected to be linked with several processes of interactions or scattering in the EAS development, and hence it contains information about the nature of the EAS initiating particle.

The LDF of electrons/muons for showers initiated by heavy primaries is generally flatter relative to that of showers initiated by lighter primaries. The steepness of the LDF or the so-called shower age in cascade theory is being used as a CR mass sensitive observable by experiments with surface detectors.

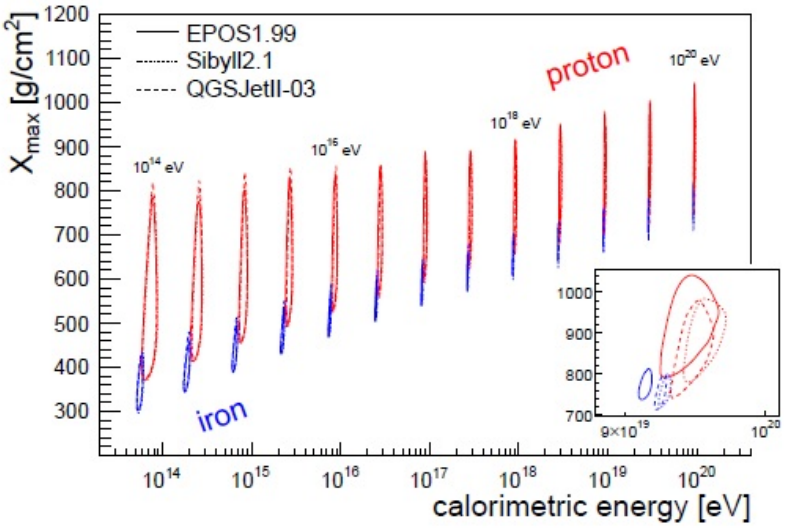

FIGURE 2.2: Simulation results of the depth of shower maximum vs. calorimetric energy. Regions shown by contour lines meaning an inclusion of 90% of the showers. The inset presents a complete view around 5×10^{20} eV (figure is taken from [6]).

2.2.2 EAS observables from longitudinal development

The EAS longitudinal development in the atmosphere contains information about the nature of the EAS initiating primary particle. Hence the measurement of appropriate EAS observables characterizing the longitudinal development of an EAS can lead to the estimation of the CR mass composition. Being a huge

medium, the atmosphere initially drives the EAS development, and later it induces atmospheric fluorescence or Cherenkov radiation, which in turn feed signals to the detector assembly on the ground. A maximum part of the EAS energy can be observed in its electromagnetic form. This form of energy drives detectors to observe the EAS development which in turn, is indeed useful for the estimation of CR energy. This electromagnetic form of energy is called calorimetric energy. A simulation study for the variation of the average depth of shower maximum with calorimetric energy is shown in Fig.2.2 [6].

The directly accessible EAS data that can be accessed from a Cherenkov detector/array, are the number density, arrival time of photons and the Cartesian and polar coordinates of each detector. On the other hand, the relevant directly accessible EAS observables that can be obtained from air fluorescence detectors are the photon density, instantaneous arrival direction of the photons and the arrival time. Using fluorescent data one has to determine the size of a shower as a function of its trajectory (from the longitudinal shower profile). All these information can then be used to derive a number of EAS observables, such as the CR energy and the depth of maximum development ($X_{\max}$). The $X_{\max}$ parameter is used to infer the nature of the CR particle. The fluctuations in $X_{\max}$ i.e. $\sigma_{X_{\max}}$ from shower-to-shower also show sensitivity to the CR particle types and hence provide interesting information about the composition of different nuclei in CRs [7].

Detection of Cherenkov or fluorescence light in an EAS is done so far in the optical range and hence requires moonless clear dark skies. This keeps duty-cycle of such systems within 10%. Detection of radio emission from EASs might give a better duty cycle for observations of showers. The radio emission in fact reflects the EAS development of leptons of the EAS. The detection techniques of radio emission in combination with particle detectors in arrays opens up a very promising technique to estimate the mass composition of CRs as well as their energy spectrum.

Temporal properties of a shower can be used as a parameter to discriminate the mass composition of CRs. Investigations over the temporal structure of EASs have been made by many authors [8–14] to give some potential observables that can be related to the primary mass composition. Muons are the best suited leptons for the purpose because they are generated from the first few interactions in the

atmosphere and they possess much longer attenuation lengths in the atmosphere and hence can easily reach to the ground level.

The reconstruction of the mean heights of production of muons in EAS brings much interest to apply it for estimating CR mass composition. The average muon charge ratio in EASs was also used as a CR mass sensitive observable in some experiments.

2.2.3 Measurements of the primary composition of cosmic rays

Analyzing directly accessible data from EAS experiments one or more observables sensitive to the mass composition of CRs are usually measured. The experimental data can then be interpreted by simulation predictions using high and low energy models for hadronic interactions. Recent measurement strategy of the nuclear composition of CRs involve multi-observable approach so that the model dependence of any estimation will be reduced significantly. The CR mass composition at energies around the *knee* region is very crucial to understand this spectral feature but it is not as well-estimated as at energies below $\approx 10^{14}$ eV. We will discuss recent measurements of the CR mass composition using data from particle detectors as well as from optical detectors.

2.2.4 N_e and N_μ method

Around *knee* energies of the energy spectrum, many experiments have performed their measurements for elemental spectra by measuring the *electron/shower* and *muon sizes* of EASs on ground, induced by CRs. The above pair of observables were used in many EAS experiments such as EAS-TOP [15], GRAPES-3 [16], KASCADE-GRANDE [17], CASA-MIA [18], AGASA [19], Yakutsk [20] and GAMMA [21] etc. At the south pole, Ice Top [22] measures high energy muons (threshold energy; $E_{\rm th.} = 500$ GeV) by using series of tanks with frozen ice whereas electromagnetic components are measured at the ground level. The EAS-TOP and MACRO at the Gran Sasso using surface detectors [23] combine their muon data with those from underground Baksan laboratory [24]. In another combination where the Tibet-ASγ [25] having array of emulsion chambers operate simultaneously with burst detectors and Telescope array [26]. In Fig.2.3, a

two-dimensional shower size distribution is shown with a more correct approach by taking all correlations into it [27]. The two-dimensional electron/shower size - muon size plot can be utilized for an unfolding analysis of KASCADE-Grade data. The KASCADE-Collaboration from the measurement of *electron* and *muon*

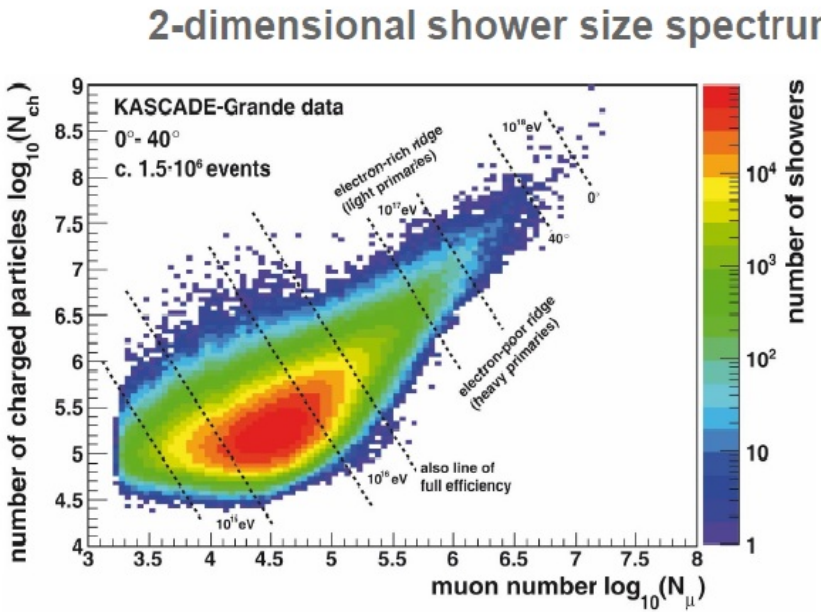

FIGURE 2.3: Distribution of the shower size vs muon size as measured by KASCADE-Grande (figure is taken from [27]).

sizes yielded a result of a light domination at the *knee* with a change towards a heavy nuclei beyond the *knee*. In [23, 28, 29], similar conclusions have been reported. In GAMMA experiment, the all-particle energy spectrum offered better tuning for a light composition near the *knee*, with a gradual increase of heavier population of nuclei beyond the *knee* while interpreted by simulation results. Results of Tibet ASγ show an early increase of nuclear composition at energies well below the *knee* and continue up to the *knee*. The KASCADE-Grande data recently indicated a very heavy composition at about energies just below the *ankle*. In Fig.2.4 the mean logarithmic atomic mass versus CR primary energy for the KASCADE-Grande in comparison with some other experiments are shown [30]. Using muon multiplicity information, GRAPES-3 experiment [31] observed significant differences between high energy hadronic interaction models SIBYLL and QGSJET.

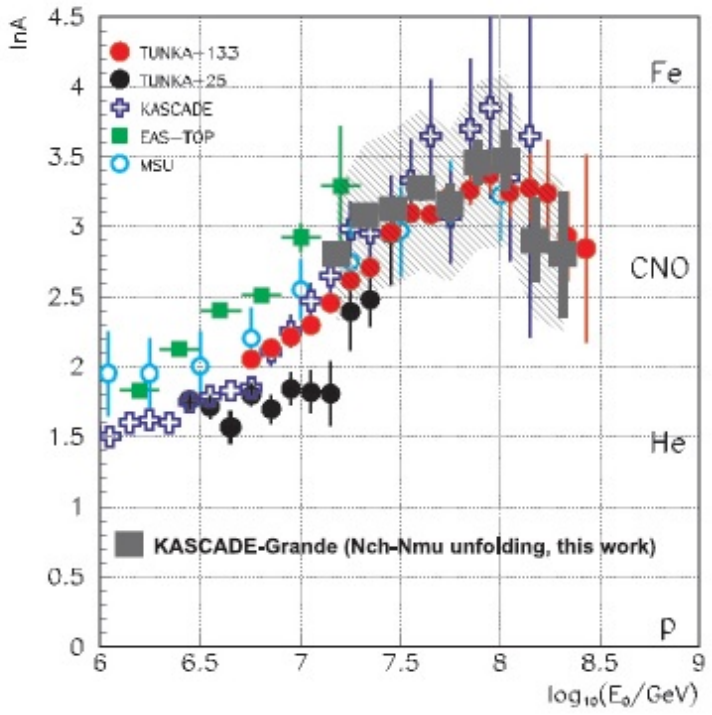

FIGURE 2.4: The mean logarithmic atomic mass as a function of the CR energy are derived from some experiment. Overlaid is the development of the mean logarithmic mass (grey, quadratic markars) computed based on QGSJET-II-02 and FLUKA 2002.4.(figure is taken from [30]).

2.2.5 Slope of the lateral distribution function

Slope of the LDF essentially describes the form or shape of the lateral density distribution (LDD) of EAS electrons/muons and is directly linked with the shower age parameter s. It also measures the degree of steepness of the LDD of particles under consideration. Generally the parameter s is obtained from the fit of the observed LDD data by any well-suited LDF. There were many analyses made using observed LDD data during the period from 1970 to 1990 for its measurement. The Mt. Norikura group [32] carried out such an analysis for the measurement of CR mass composition using the parameter and they hinted a transition from lighter to heavier domination beyond a shower size $\approx 10^7$ [33]. The analysis of Akeno data [34] indicated an increase in s with increasing muon size at fixed shower sizes. Recently the ARGO-YBJ group measured the sensitivity of the LDD shape parameter within few meters around the core to the nature of the EAS initiating primary particle. Their results suggest the possibility of using the lateral shower age or slope of the LDF, for the estimation of the CR mass

composition [35].

There exists one more slope parameter as predicted in the electro-magnetic cascade theory which actually determines the evolving stage of pure EM cascades. The parameter is expressed by the longitudinal shape or shower age $s_{\parallel}$ parameter. The $s_{\parallel}$ parameter can be estimated observationally only if EAS experiment is equipped with Cherenkov or fluorescence detectors.

2.2.6 Muon production heights

Reconstruction of the average muon production height in EAS appeared as a promising technique with the CR tracking detectors at HEGRA, the muon tracking detector at KASCADE or GRAPES. Measuring the orientation of the muon track with respect to the EAS axis the muon production height can be reconstructed. The KASCADE-Grande measurements of the muon production height is well-suited with a clear transition from proton/helium dominated to iron dominated CR nuclei across the *knee* energies [36].

2.2.7 Rise-Time

The CR mass composition can also known from time profile of EAS particles particularly in the UHE region. Haverah Park experiment [37] used such timing information of EAS particles for studying mass composition of CRs and hinted a transition from a light to heavy in the energy interval $3 \times 10^{18} - 4 \times 10^{19}$ eV.

2.2.8 Non-imaging Cherenkov and Fluorescent measurements

Observations of Cherenkov light from EAS was first detected by the AIROBICC detectors installed at HEGRA and CASA-BLANCA [38] in Utah. In the UHE region the Tunka [39] and Yakutsk [40] exploited the same technique to measure the depth of shower maximum parameter of EAS. Experiments like LOFAR and Pierre Auger observatory (PAO) were also engaged for the CR mass composition measurement much beyond the *knee* with the help of the parameter $X_{\max}$ from fluorescence measurements. This measurements aim to reconstruct the longitudinal development of the EAS as a function of slant depth. Generally, the

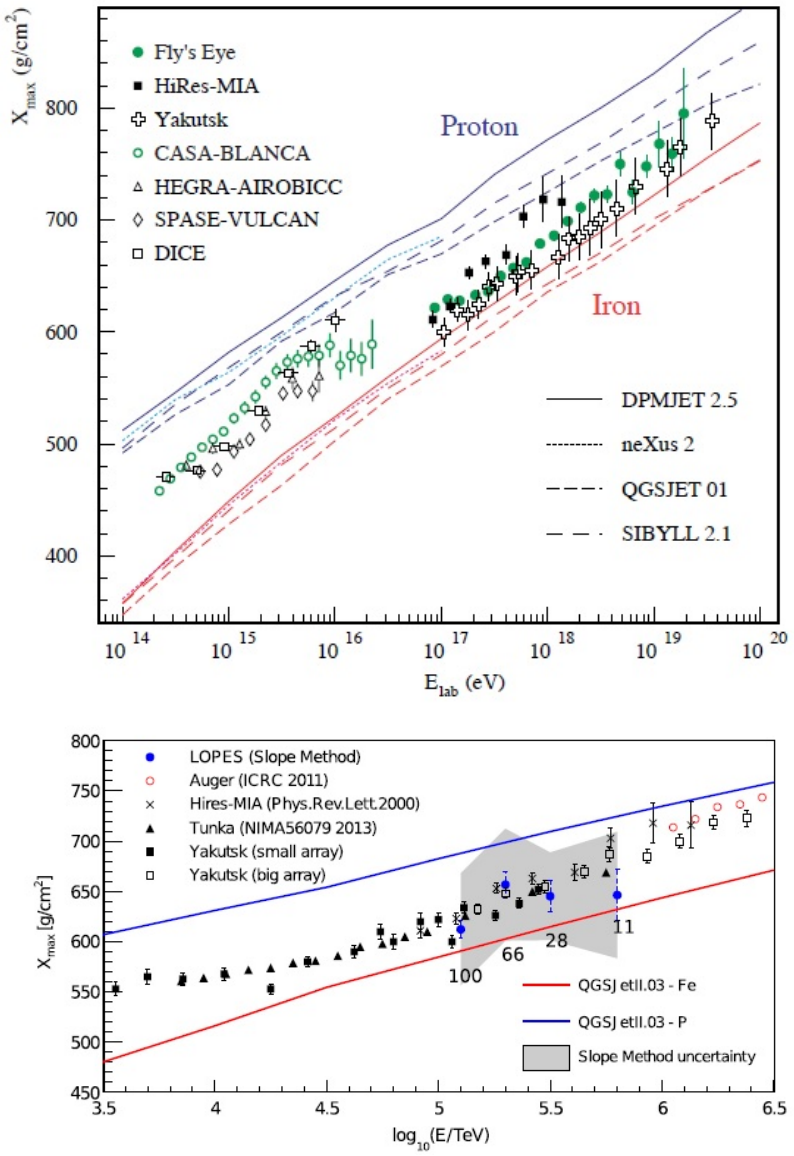

FIGURE 2.5: Top: Compilation of several experimental results for the estimation of X_{max} by measuring the air Cherenkov light(Yakutsk [41], BLANKA [42], HEGRA [43], TUNKA-25 [44], SPASE [45], CACTI [46], DICE [47]). Monte Carlo simulations for two different models are also shown; Bottom: Same as above but LOPES and Auger results were derived from radio and fluorescence data.

distribution of different values of $X_{\max}$ corresponding to a small primary energy interval contains a reasonable information about the CR mass composition from fluorescence detector signals. In Fig.2.5 a variation of the mean $X_{\max}$ with the CR energy from different experiments compared with simulation results is depicted. The systematic of $X_{\max}$ i.e. $\sigma X_{\max}$ as well as the muon production depth from Auger are compatible to an idea of gradual transition from lighter towards a heavier composition in the UHE region. But, the nature of $X_{\max}$ variations for HiRes, Telescope Array [26] indicate a lighter CR mass composition in this EeV

regions.

2.2.9 Radio measurements

Recently the detection of coherent radio emission from EASs has been made by many experiments [48]. A more accurate measurement of $X_{\max}$ of EASs with higher duty cycle from radio detection technique is a primary objective of these experiments. In these measurements $X_{\max}$ parameter of EASs can be estimated either from characteristics of the lateral distribution of radio signals or from features of the shape of the radio wave front. $X_{\max}$ is treated as an important indicator for CR mass composition study and this was reconstructed more accurately by LOPES experiment using the first method [49]. The parameter was found effective for the reconstruction of primary energy as well using LOPES data.

Table 2.1 compiles the EAS experiments done throughout the globe with their observable parameters.

2.3 Summary

It has been realized that a variety of experimental techniques is applied at least to gain some qualitative understanding of the CR mass composition. These techniques involve different types of detectors and they ultimately contribute a wealth of new data which in turn provide a lot of EAS observables sensitive to the CR mass composition. In the energy range, $10^{14} - 10^{17}$ eV, information such as electron number, muon number or even hadron number of an EAS have yielded many interesting results on the CR mass composition. Non-imaging Cherenkov measurements of an EAS have also contributed to the understanding of the mass of CRs. Beyond 10^{17} eV the fluorescence measurements have been proven successful for the purpose.

It is believed that a concrete understanding of the first spectral structure at around $\approx 3 - 4$ PeV might provide some insight on the origin of the galactic CRs. In the PeV region the average mass of CRs is found to increase with energy predicted by most of the experiments operated in the region. For detailed understanding of the origin of the *knee*, a more accurate estimation of the CR mass composition

TABLE 2.1: EAS experiments done so far

Experiments	Detector	Observables	Location	References
KASCADE	Scint.array	N_e, N_μ	Karlsruhe	[50]
	LST-tunnel	μ tracking	Germany	[51]
	Calorimeter	N_h, E_h	E8.4 N49.0	[52]
	MWPC,LST,	N_μ, ρ_μ		[53]
	Scint.	μ-arrival times		
KASCADE-Grande	Scint. array	N_{ch}		[54]
EAS-TOP	Scint. array	N_e	Gran Sasso	[55]
	$h-\mu-calorimeter$	N_μ, h	Italy	
AKENO	Scint. array	N_e	Akeno, Japan	[56]
	μ-counter	N_μ	E138.5 N35.8	[57]
	C -counter	X_{max}		
TIBET-ASγ	Scint. array	N_e	Yanbajing , China	[58]
CASA	Scint. array	N_e	Dugway,	[59]
MIA	μ-underground	N_μ	Utah, US	[60]
BLANCA	C-light	X_{max}	W112.8	[61]
DICE	2 imag.C-telescope	X_{max}	N40.2	[62]
Yakutsk	Scint. array	N_e, N_μ	Russia	[63]
	C-light	X_{max}	E 129.4,N61.7	
	μ-underground			
AUGER	Water C-array	N_e, N_μ	Argentina	[64]
	FD -telescope	Flour. light	W69.3	
			S 35.5	
GRAPES-III	Scint.array	N_e	Ooty , India	[65]
	Prop.counters	N_μ		
Tien-Shan	Scint.array	N_e	Kyrgyzstan	[66]
	C-light	X_{max}		
Tunka13	C-light	X_{max}	Russia	[67]
			E103,N51.5	

is necessary. In this context, involvement of several EAS observables in a multi-observable approach, from relatively new shower data analysis techniques may deliver a more accurate estimate of the CR mass composition.

It should be however mentioned that the inference on the mass composition from the CR observed data is presently limited by the uncertainties in the hadronic interaction models used in the air shower simulation. There is a relentless effort to make the hadronic interaction models more reliable by latest accelerator data. On the other hand, efforts to be given to maintain a better consistency between hadronic interaction models and EAS measurements particularly in the UHE region [68].

Bibliography

[1] Ginzburg V. L. and S. I. Syrovatskii, *Pergamon press*, Oxford (1964).

[2] The Pierre Auger Collaboration, *Phys. Lett. B*, **685**, 239 (2010).

[3] The Pierre Auger Collaboration, *Phys. Rev. Lett.*, **101**, 061101 (2008).

[4] Telescope Array Collaboration, *Astrophys. J.*, **768**, L1 (2013).

[5] KASCADE collaboration, *Astropart. Phys.*, **24**, 1, (2005).

[6] Karl-Heinz Kampert and Michael Unger, *Astropart. Phys.*, **35**(10) 660 (2012).

[7] V. Berezinsky *et al.*, *Phy. Rev. D*, **74**, 043005 (2006).

[8] Rebel, H., *et al.*, *J. Phys. G*, **21**, p. 451 (1995).

[9] Brancus, I.M., *et al.*, *Astropart. Phys.*, **7**, p. 343 (1997).

[10] Brancus, I.M.,*et al.*, *J. Phys. G*, **29**, p. 453 (2003).

[11] Blake, P.R., and W.F. Nash : *J. Phys. G*, **24**, p. 217 (1998).

[12] Antoni, T.,*et al.*, *Astropart. Phys.*, **15**, p. 149 (2001b).

[13] Antoni, T.,*et al.*, *Astropart. Phys.*, **18**, p. 319 (2003a).

[14] Haeusler, R.,*et al.*, *Astropart. Phys.*, **17**, p. 421 (2002).

[15] M. Aglietta *et al.*, *Nucl. Instrum. Methods*, A**336**, 310 (1993).

[16] S. Gupta *et al.*, GRAPES-3 collaborations, *Nucl. Instrum. Methods*, A**540**, 311 (2005).

[17] W. Apel *et al.*, KASCADE-Grande collaborations, *Nucl. Instrum. Methods*, A**620**, 202 (2010).

[18] A. Borione *et al.*, CASA-MIA collaborations, *Nucl. Instrum. Methods*, A**346**, 329 (1994)

[19] N. Chiba *et al.*, *Nucl. Instrum. Methods*, A**311**, 338 (1992).

[20] B.N. Afanasiev *et al.*, in: Proceedings Tokyo Workshop on Techniques for the Study of EHECRs, p. 35 (2003).

[21] A. Garyaka *et al.*, GAMMA collaborations, *Astropart. Phys.*, **28**, 169 (2007).

[22] A. Achterberg *et al.*, Ice-Cube collaborations, *Astropart. Phys.*, **26**, 155 (2006).

[23] M. Aglietta *et al.*, EAS-TOP and MACRO Collaborations, *Astropart. Phys.*, **20**, 641 (2004).

[24] V. Bakatanov *et al.*, *Astropart. Phys.*, **12**, 19 (1999).

[25] A. Amenomori *et al.*, Tibet ASc Collaborations, *Astroph. J.*, **678**, 1165 (2008).

[26] J. Matthews *et al.*, TA Collaborations, in: *Proceedings 32nd ICRC.*, vol. 2, p. 273 (2011).

[27] W. D. Apel *et al.*, *Phys. Rev. Lett.*, 107.171104 (2011).

[28] M. Glasmacher *et al.*, *Astropart. Phys.*, **10**, 291 (1999).

[29] S. Swordy *et al.*, *Astropart. Phys.*, **18**, 129 (2002).

[30] S.F. Berezhnev *et al.*, Tunka-133: Primary: *In Proc. 32nd ICRC.*, Beijing (2011).

[31] S K Gupta *et al.*, *Nucl. Instrum. Methods*, A **540**, 311 (2005).

[32] Miyake S *et al.*, *PICRC*,**5**, p.3220 (1973).

[33] Miyake S *et al.*, *PICRC*,**13**, p.171 (1979).

[34] Hara T*et al.*, *PICRC*, **11**, 231 (1981).

[35] B. Bertoli *et al.*, *Astropart. Phys.*, **93**, 46 (2017).

[36] W. D. Apel *et al.*, *Asropart. Phys.*, **34**, 476 (2011).

[37] R. Walker, A. A. Watson : *J. Phys. G*, **8**, 1131 (1982).

[38] J. W. Fowler et al., Astropart. Phys. 15 (2001), 49–64, astro-ph/0003190

[39] N. Budnev *et al.*, Tunka collaborations, *Nucl. Phys. (Proc. Suppl.)*, **190**, 247 (2009).

[40] S. Knurenko, A. Sabourov, in: *Proceedings 32nd ICRC.*, vol. 1, p. 189 (2011)

[41] Efimov N N *et al.*, Proc. Int. Symp. Astrophysical Aspects of the Most Energetic Cosmic Rays ed M Nagano and F Takahara, p 20 (1991)

[42] Fowler J W *et al.*, *Astropart. Phys.*, **15**, 49 (2001)

[43] Arqueros F *et al.*, *Astron. Astrophys.*, **359**, 682 (2000)

[44] Prosin V V *et al.*, 2002 Private communication

[45] Dickinson J E *et al.*, *Proc. 26th Int. Cosmic Ray Conf.*, (Salt Lake City) vol 3, p 136 (1997)

[46] Paling S *et al.*, *Proc. 25th Int. Cosmic Ray Conf.*, (Durban) vol 5, p 253 (1997)

[47] Boothby *et al.*, *Astrophys. J.*, **491**, L35 (1997)

[48] H. Falcke *et al.*, *Nature Letts.*, **435**, 313 (2005)

[49] W. D. Apel *et al.*, *Phys. Rev. D*, **90**, 062001 (2014)

[50] Antoni T *et al.*, KASCADE Collaboration *Nucl. Instrum. Methods*, A at press Klages H O *et al.*, 1997 *Nucl. Phys. (Proc. Suppl.)*, B **52**, 92 (2003)

[51] Doll P *et al.*, *Nucl. Instrum. Methods*, A **488**, 517 (2002)

[52] Engler H *et al.*, *Nucl. Instrum. Methods*, A **427**, 528 (1999)

[53] Bozdog H *et al.*, *Nucl. Instrum. Methods*, A **465**, 455 (2001)

[54] Bertaina M *et al.*, *Proc. 27th Int. Cosmic Ray Conf.*, (Hamburg) vol 2, p 792 (2001)

[55] Aglietta M *et al.*, *Nucl. Instrum. Methods*, A **277**, 23 (1989)

[56] Nagano M *et al.*, *J. Phys. G: Nucl. Part. Phys.*, **10**, 1295 (1984)

[57] Teshima M *et al.*, *Nucl. Instrum. Methods*, A **311**, 338 (1992)

[58] Amenomori M *et al.*, *Astrophys. J.*, **461**, 408 (1996)

[59] Glasmacher M *et al.*, *Astropart. Phys.*, **10**, 291 (1999)

[60] Borione A *et al.*, *Nucl. Instrum. Methods*, A **346**, 682 (2000)

[61] Fowler J W *et al.*, *Astropart. Phys.*, **15**, 49 (2001)

[62] Swordy S and Kieda D : *Astropart. Phys.*, **13**, 137 (2000)

[63] Afanasiev N N *et al.*, *Proc. 24th Int. Cosmic Ray Conf.*, (Rome) vol 2, p 756 (1995)

[64] Pierre Auger Project Design Report 1997, Pierre Auger Collaboration, Fermi National Accelerator Lab. www.auger.org/admin
Dova M T *et al.*, Pierre Auger Observatory Collaboration, *Proc. 27th Int. Cosmic Ray Conf.*, (Hamburg) vol 2, p 699 (2001)

[65] Hayashi Y *et al.*, *Proc. 27th Int. Cosmic Ray Conf.*, (Hamburg) vol 1, p 111 (2001)

[66] Antonov R A *et al.*, *Proc. 27th Int. Cosmic Ray Conf.*, (Hamburg) vol 2, p 828 (2001)

[67] Gress O A *et al.*, *Nucl. Phys. (Proc. Suppl.)*, B **75**, 299 (1999)

[68] D. Allard *et al.*, *Astron. and Astrophys.*, **473(1)**, 59 (2007)